PLOS ONE

RESEARCH ARTICLE

Thy1 transgenic mice expressing the red fluorescent calcium indicator jRGECO1a for neuronal population imaging *in vivo*

Hod Dana[1¤], Ondrej Novak[1,2], Michael Guardado-Montesino[1], James W. Fransen[3], Amy Hu[1], Bart G. Borghuis[3], Caiying Guo[1], Douglas S. Kim[1], Karel Svoboda[1]*

1 Janelia Research Campus, Howard Hughes Medical Institute, Ashburn, VA, United States of America, **2** Department of Auditory Neuroscience, Institute of Experimental Medicine, Academy of Sciences of the Czech Republic, Prague, Czech Republic, **3** Department of Anatomical Sciences and Neurobiology, University of Louisville School of Medicine, Louisville, KY, United States of America

¤ Current address: Department of Neurosciences, Lerner Research Institute, Cleveland Clinic Foundation, Cleveland, OH, United States of America
* svobodak@janelia.hhmi.org

Citation: Dana H, Novak O, Guardado-Montesino M, Fransen JW, Hu A, Borghuis BG, et al. (2018) *Thy1* transgenic mice expressing the red fluorescent calcium indicator jRGECO1a for neuronal population imaging *in vivo*. PLoS ONE 13 (10): e0205444. https://doi.org/10.1371/journal.pone.0205444

Editor: Tudor C. Badea, National Eye Centre, UNITED STATES

Received: June 18, 2018

Accepted: September 25, 2018

Published: October 11, 2018

Data Availability Statement: Lines GP8.20, GP8.31, GP8.58 and GP8.62 are available at The Jackson Laboratory (http://jaxmice.jax.org), with stock numbers 030525, 030526, 030527, and 030528, respectively. AAV for jRGECO1a expression are available at the University of Pennsylvania Vector Core (http://www.med.upenn.edu/gtp/vectorcore/Catalogue.shtml). High-resolution confocal microscopy images of lines GP8.20, GP8.31, GP8.58 and GP8.62 are available

Abstract

Calcium imaging is commonly used to measure the neural activity of large groups of neurons in mice. Genetically encoded calcium indicators (GECIs) can be delivered for this purpose using non-invasive genetic methods. Compared to viral gene transfer, transgenic targeting of GECIs provides stable long-term expression and obviates the need for invasive viral injections. Transgenic mice expressing the green GECI GCaMP6 are already widely used. Here we present the generation and characterization of transgenic mice expressing the sensitive red GECI jRGECO1a, driven by the *Thy1* promoter. Four transgenic lines with different expression patterns showed sufficiently high expression for cellular *in vivo* imaging. We used two-photon microscopy to characterize visual responses of individual neurons in the visual cortex *in vivo*. The signal-to-noise ratio in transgenic mice was comparable to, or better than, mice transduced with adeno-associated virus. In addition, we show that *Thy1*-jRGECO1a transgenic mice are useful for transcranial population imaging and functional mapping using widefield fluorescence microscopy. We also demonstrate imaging of visual responses in retinal ganglion cells *in vitro*. *Thy1*-jRGECO1a transgenic mice are therefore a useful addition to the toolbox for imaging activity in intact neural networks.

Introduction

Imaging calcium dynamics with genetically encoded calcium indicators (GECIs) is commonly used for measuring activity of neuronal populations and also in subcellular compartments. For example, two-photon imaging of GCaMP6 has been used to monitor the activity of thousands of neurons in behaving rodents [1–3]. jRGECO1a is a recently developed red fluorescent GECI with high sensitivity and fast kinetics. jRGECO1a can report action potential (AP) firing in flies, fish, worms, and mice [4, 5]. In mice, jRGECO1a can be expressed stably for months and can be used together with green GECIs to study interactions between multiple neuronal populations in separate color channels.

at FigShare (https://doi.org/10.6084/m9.figshare.7117544.v1).

Funding: HD, ON, MGM, AH, CG, DSK, and KS were supported by the Howard Hughes Medical Institute Janelia Research Campus, as part of their budget to the GENIE Project. The funders had no role in study design, data collection and analysis, decision to publish, or preparation of the manuscript. JWF and BGB were supported by the National Institute of Health National Eye Institute by grant number R01-EY028188. The funders had no role in study design, data collection and analysis, decision to publish, or preparation of the manuscript.

Competing interests: The authors have declared that no competing interests exist.

GECIs can be introduced into the brain by injection of adeno-associated virus (AAV), or integration of a transgene containing a neuronal promoter and GECI cDNA into the genome of mice [6–8]. AAVs readily produce the high intracellular GECI concentration (~ 10 – 100 μM) required for *in vivo* imaging, in an area of several hundred micrometers around the injection site [9–11]. However, the expression is spatially inhomogeneous, with the highest concentration found near the injection site. Moreover, expression levels gradually increase with time, and overexpression can cause aberrant neural activity [12, 13]. The time window for AAV-mediated GECI imaging is thus limited by increasing GECI expression level, which depends on the promoter strength, viral titer, injection volume, and other factors. Finally, AAV-mediated gene transfer requires additional invasive surgeries [9].

GECI expression in transgenic mice is stable over extended periods [6, 11, 14, 15], potentially even the entire life of the mouse. Expression patterns and levels are reproducible across different individual animals [6, 11]. Multiple transgenic GECI lines have been developed using different transgene insertion techniques [6–8, 11, 14–23]. Cre recombinase-responsive reporter lines can be used in combination with Cre-expressing driver lines to flexibly express GECIs in specific cell types. However, this scheme requires breeding of two transgenic mouse lines. In addition, using the Cre system to drive GECI expression, will not allow using it to drive expression of other proteins, such as optogenetic effectors. Transgenic mouse lines expressing GECIs under the *Thy1* promoter provide a powerful alternative for imaging projection neurons across the mouse brain [6, 24]. We developed transgenic mouse lines expressing the jRGECO1a GECI under the *Thy1* promoter [21, 25, 26]. We characterized the brain-wide expression patterns of each line and show that these mouse lines are useful for functional imaging using two-photon microscopy and widefield fluorescence imaging.

Materials and methods

All surgical and experimental procedures were in accordance with protocols reviewed and approved by the Janelia Research Campus Institutional Animal Care and Use Committee and Institutional Biosafety Committee (protocol #16–135), as well as the Institutional Animal Care and Use Committee at the University of Louisville (protocol #16717).

Transgenic mice

We report on Janelia Research Campus GENIE Project (GP) lines GP8.x (where 'x' refers to the founder number) expressing jRGECO1a for neural activity imaging. *Thy1*-jRGECO1a-WPRE transgenic mice were generated using C57BL6/J mice [27]. The transgene includes the *Thy1* promoter [21], a nuclear export signal (NES; from cAMP-dependent protein kinase inhibitor alpha subunit) fused upstream of jRGECO1a, a woodchuck hepatitis virus post-transcriptional regulatory element (WPRE) that has been shown to increase mRNA stability and protein expression [28, 29], and a polyadenylation signal (pA) from the bovine growth hormone gene. Genotyping primers were `5′-ACAGAATCCAAGTCGGAACTC-3′ and 5′-CCTATAGCTCTGACTGCGTGAC-3′`, which amplify a 296-bp fragment spanning part of the *Thy1* promoter and NES-jRGECO1a. Mouse lines GP8.20, GP8.31, GP8.58, and GP8.62 were deposited at The Jackson Laboratory (stock no. 030525, 030526, 030527, 030528).

Analysis of jRGECO1a expression

Mice were held in standard housing cages with *ad libitum* access to food and water. Adult mice (P42-P56, n = 76 mice) were deeply anesthetized with isoflurane, perfused with PBS and paraformaldehyde, and their brains were processed for immunohistochemistry as described in [6]. Native jRGECO1a fluorescence was imaged using a panoramic digital slide scanner

(3DHISTECH) (S1 Data). For a subset of mouse lines (GP8.20, GP8.31, GP8.58, GP8.62) we performed NeuN immunostaining on sections [30]. Coronal sections were blocked with 2% BSA and 0.4% Triton X-100 solution for 1 hour at room temperature to prevent nonspecific antibody binding, and then sections were incubated overnight at 4˚C with mouse anti-NeuN primary antibody (1:500; Millipore, MAB 377). Sections were then incubated with Alexa Fluor 488-conjugated goat-anti-mouse secondary antibody (1: 200; Life Technologies, A11032) for 4 hours at room temperature. Brain sections were mounted on microscope slides with Vecta-shield mounting medium (H-1400, Vector laboratories).

Confocal images (LSM 800, Zeiss) were collected for selected brain regions, using an 20x 0.8 NA objective and standard mCherry imaging filters. Individual images were tiled and stitched by the microscope software (Zeiss). We analyzed anterior lateral motor cortex (ALM), primary motor cortex (M1), primary somatosensory cortex (S1), primary visual cortex (V1) and hippocampus (CA1, CA3, and dentate gyrus, DG). For sample regions in each area we identified all labeled cells, regardless of the labeling brightness, segmented their somata and calculated the somatic jRGECO1a fluorescence brightness for each cell. Neocortical cells were grouped into layer 2/3 and layer 5 cells. We also counted the proportion of all the jRGECO1a labeled cells (red channel; weakly and strongly labeled cells were grouped together) as the number of jRGECO1a positive cells over the number of NeuN positive cells (green channel; all labeled cells were counted). To compensate for variations of imaging conditions across time (e.g. changes in the excitation light source intensity), images of 3.8 μm fluorescent beads (Ultra Rainbow Fluorescent Particles, Bangs Laboratories) were acquired and the average bead brightness was used to normalize the jRGECO1a signal.

In addition, we performed a coarse analysis of expression levels across numerous brain regions, based on widefield images of coronal sections (Table 1; S1 Data).

Table 1. Brain wide jRGECO1a expression of multiple GP lines.

Line	ALM	M1	Piriform area	Amygdala	S1	Hippo-campus	Thalamus	Hypo- thalamus	V1	Mid-brain	Pons	Retina
8.5	++	++	+++	++	+	+++	-	-	+	-	+	++
8.7	+	+	+	+	+	++	+	-	+	+	++	+
8.8	+	+	+	+	+	++	-	-	+	-	-	-
8.20	+++	+++	+++	+	+++	+++	++	-	+++	+	+	+
8.24	+	+	+	+	+	+	+	-	+	-	-	+
8.26	+	+	-	-	+	+	-	-	+	-	-	_
8.27	+	+	-	+	+	++	+	-	+	-	-	_
8.30	+	+	-	+	+	++	+	-	+	-	-	_
8.31	+++	+++	+	+++	+++	+++	++	+	+++	+	+	-
8.37	+	+	+	-	+	+	-	-	+	-	+	-
8.40	+	+	++	-	+	++	-	-	+	-	-	-
8.46	++	++	++	+	++	++	+	+	++	+	+	+
8.50	++	++	++	-	++	+++	+	-	++	-	-	-
8.52	+	+	+	-	+	++	+	-	+	-	-	N/A
8.58	+++	+++	+	++	+++	+++	+	-	+++	+	+	+
8.62	+++	+++	+++	+	+++	+++	-	-	+++	+	+	-
8.64	+	+	++	++	+	++	+	-	+	-	+	-
8.66	+++	+++	+	+	+++	+++	+	-	+++	+	+	N/A

jRGECO1a brightness in multiple brain regions was qualitatively estimated based on visual inspection of widefield microscope images of coronal sections.
- no signal, + weak signal, ++ moderate signal, +++ strong signal, N/A not tested.

https://doi.org/10.1371/journal.pone.0205444.t001

Two-photon imaging in visual cortex

Mice were held in standard housing cages with *ad libitum* access to food and water. Headbars and cranial windows were implanted in 2–8 months old GP8 mice (n = 8 mice). Mice were anesthetized with isoflurane (2.5% for induction, 1.5% during craniotomy and headbar implantation) [6]. Mice were injected with chlorprothixene hydrochloride (30 μl of 0.33mg/ml solution, i.m., Sigma) and kept lightly anesthetized during imaging (0.5% isoflurane). Imaging was performed immediately after completing the craniotomy, and the mice were euthanized at the end of the experiment by deep anesthesia (5% isoflurane) followed by cervical dislocation. Imaging was performed using a custom-built two-photon microscope with a resonant scanner. The light source was an Insight DS+ laser (Spectra-Physics) running at 1100 nm. The objective was a 16x water immersion lens with 0.8 NA (Nikon). Images were acquired using ScanImage 5 (vidriotechnologies.com). Images (512x512 pixels, 250x250 μm^2; 100–250 μm below the pia) were collected at 29 Hz. Laser power was 50–140 mW at the brain surface. Mice were presented with 1Hz sinusoidal drifting grating stimuli, moving in 8 different directions. The signal analysis was similar to our previous characterization studies [4, 6, 13] and was performed in Matlab (Mathworks). In short, all visible cell bodies were segmented using a semi-automated algorithm. Neuropil contamination was corrected with r = 0.7, as described in [6], baseline signal for $\Delta F/F_0$ calculations was estimated by averaging the 700ms prior to the start of the stimulus. Cells with significant increase in their fluorescence signal during stimulus presentation were identified using an ANOVA test (P = 0.01). The half decay time was calculated for significantly responsive cells with response amplitude larger than 4 standard deviations of the baseline signal above the baseline signal level.

For quantifying AAV-mediated expression of jRGECO1a, two adult C57BL6/J mice (P42-56) were anesthetized and injected with AAV-*synapsin-1*-NES-jRGECO1a (AAV-jRGECO1a) into the primary visual cortex (2 injections, 25 nl each, centered 2.5 and 2.9 mm left, and 0.2 mm anterior to Lambda suture) using standard protocols [13]. 45–60 days after viral injection the mice were perfused and coronal sections were cut and imaged. Images were analyzed the same way like *Thy1*-jRGECO1a expression data. Functional activity data for AAV-jRGECO1a mice were taken from [4], and was acquired under the same experimental conditions.

Widefield imaging through the intact skull

Mice were held in standard housing cages with *ad libitum* access to food and water. Young adult mice (P35-42, n = 5 mice) were anesthetized with isoflurane (2.5% for induction and 1.5% during surgery) in oxygen and placed onto a heated pad (37˚C). Buprenorphine HCl (0.1 mg/kg) and ketoprofen (5 mg/kg) were administered for analgesia, and ketoprofen was also administered 24 and 48 hours after the surgery. A flap of skin covering frontal and parietal bones was removed using a scalpel. The skin margins were glued to the skull bone (Loctite, Ultra Gel Control Super Glue), leaving the left parietal bone, and the left part of the interparietal bone exposed. A custom-made titanium head bar was glued and cemented over the frontal bones and the right parietal bone of the animal. We then applied a thin layer of glue onto the remaining exposed bone covering the visual cortex. The cured glue was covered with clear nail polish (EMS #72180)[31].

Mice were imaged one week after the surgery and were anesthetized after the required data was acquired, using deep anesthesia (4% isoflurane) followed by cervical dislocation. Awake mice were head-restrained under a custom-made fluorescence microscope equipped with an Orca Flash 4.0 V3 scientific CMOS camera (Hamamatsu). To reduce stress, mice were given a droplet of water with honey after the head fixation. The brain under the intact skull overlying the left visual cortex was imaged with a 4x NA 0.2 objective (Thorlabs). An LED light source

(Mightex; center wavelength 525 nm) and a filter cube (excitation filter 535/40 nm, dichroic 585 nm, 630/75 nm emission filter) were used to excite and collect the fluorescence signal. Visual stimuli were delivered from a screen positioned approximately 15 cm in front of the animal's right eye covering angles from -10 to 100 degrees (azimuth) and -45 to 45 degrees (elevation). Twenty drifting checkerboard stimuli (6 degrees/s) were presented for each of four directions [32].

The signal from each pixel was processed using Fourier analysis. The baseline (B) was calculated as the average fluorescence before each presentation of the drifting bar stimulus. The relative changes in the fluorescence signal elicited by the visual stimulation were then calculated as (F-B)/B. The phase of the Fourier-transformed signal in a band corresponding to the stimulus repetition frequency (0.05 Hz) was computed and associated with the known position of the drifting bar. The spectral power in the same band was used to set the transparency of the retinotopy map (weaker power → more transparent).

Two-photon imaging of light-evoked responses in the retina

Mice were held in standard housing cages with *ad libitum* access to food and water. Mice were deeply anesthetized with isoflurane, euthanized by cervical dislocation, and whole-mount retinae were prepared for *in vitro* recording using established methods (n = 23 mice) [33]. Two-photon excitation was produced with a Ti:Sapphire laser (Chameleon Ultra II, Coherent) tuned to 1040 nm; fluorescence responses were detected using a 60x, 1.0 N.A. objective lens (Olympus) and conventional photomultiplier tubes (R3896; Hamamatsu). Visual stimuli were generated with Matlab (Mathworks) and the Psychophysics Toolbox (psychtoolbox.org) and presented using a video projector (HP Notebook Companion; HP) modified to project UV light (λ_{peak} = 395 nm; NC4U134A LED; Nichia, Japan), focused onto the photoreceptors using the microscope condenser. Data were analyzed with custom scripts in Matlab.

Results

jRGECO1a brain expression in *Thy1*-jRGECO1a mouse lines

We screened 18 transgenic lines of *Thy1-jRGECO1a* mice (Fig 1A, S1 Data). In *Thy1* transgenic mice, expression patterns are strongly dependent on the transgene cassette integration site in the genome [21, 25]. Expression pattern differed greatly across lines, as summarized in Table 1. But expression patterns were similar across different individual mice from the same line (S1 Fig, S1 Data) and across the F0 (founder), F1, and F2 generations. Four lines (GP8.20, GP8.31, GP8.58, and GP8.62) showed high and dense expression levels, with diverse labeling patterns across the brain. Expression was mainly limited to glutamatergic pyramidal neurons, with no apparent labeling in glia, as is typical for Thy1 transgenic mice. The expression patterns of these four lines were analyzed in more depth (Figs 1B and 1C and 2).

We quantified expression across brain regions (Table 1; S1 Data) and individual neurons by measuring integrated somatic jRGECO1a fluorescence in fixed tissue (Fig 2A). We compared the transgenic expression level to somatic signal from two C57BLl/6J mice injected with AAV-jRGECO1a in V1 area, 45–60 days post-infection (Fig 2B and 2C, S2 Fig). Neocortical AAV-mediated jRGECO1a expression was slightly higher than in *Thy1*-jRGECO1a mice. The four GP lines showed expression in overlapping brain regions; differences were due to expression levels in specific brain regions (Fig 2B–2D, Table 1). The highest expression in the GP lines was seen in the hippocampus. For neocortical regions, expression in layer 5 was typically higher than for layer 2/3 (Fig 1B and 1C and 2A–2D). Expression in layer 4 cells was absent in all lines except line GP8.20, which has dense and bright labeling in layer 4 (Fig 1B and 1C, S2

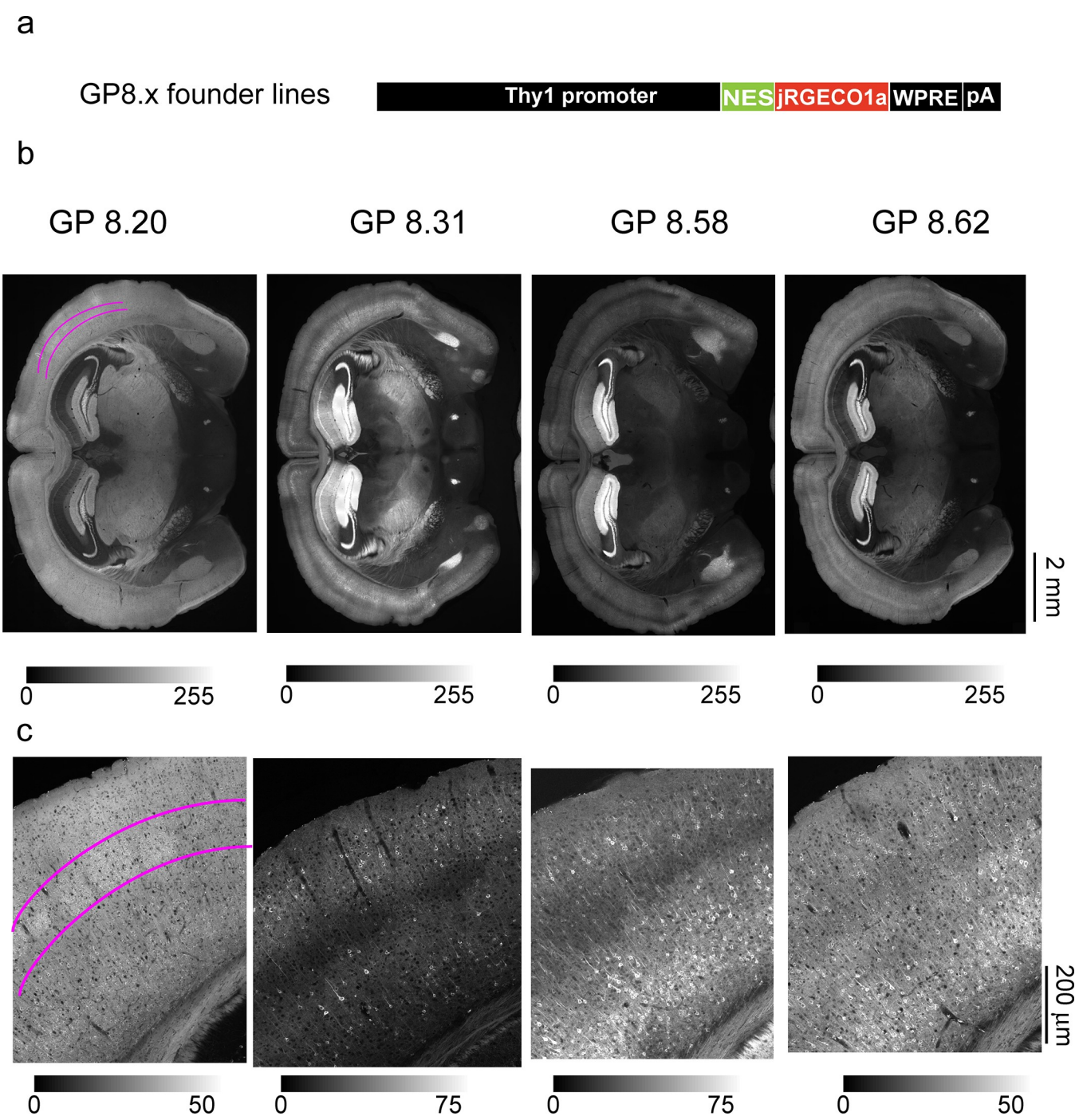

Fig 1. Expression of jRGECO1a in *Thy1*-jRGECO1a mouse lines. a. Schematic of the transgene cassette used to generate GP8.x lines. **b**. Fluorescence widefield images of coronal sections from four transgenic lines showing jRGECO1a fluorescence. Magenta marks on the GP8.20 image indicate the location of labeled layer 4 cells (see also S2 Fig). **c**. Representative confocal images (tiled and stitched to show larger field of view) from the somatosensory cortex of the same lines as in **b**.

https://doi.org/10.1371/journal.pone.0205444.g001

Fig). Expression was detected in multiple other brain regions (Table 1; S1 Data). For example, expression was high in the amygdala in several transgenic lines (Table 1).

NeuN immunostaining was used to detect all neurons [30] and thus estimate the proportion of jRGECO1a-positive neurons in several brain regions for lines GP8.20, GP8.31, GP8.58,

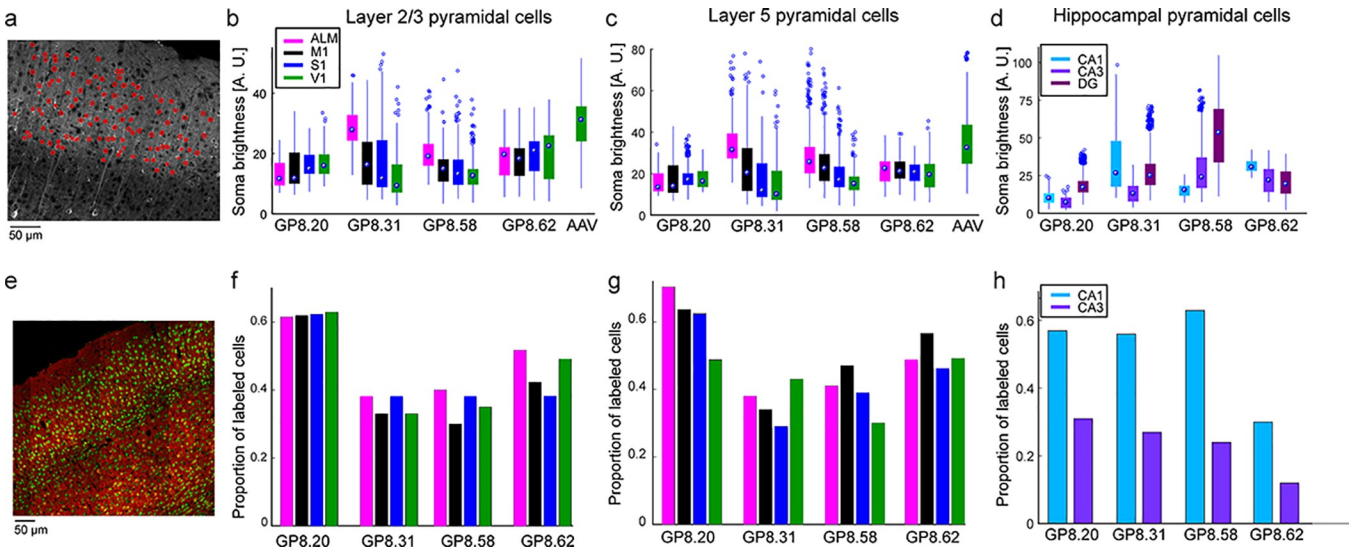

Fig 2. Quantification of jRGECO1a expression. a. Analysis method used for calculating the brightness of single neurons across brain regions. Confocal microscopy images of fixed brain slices were used for segmentation of cell bodies (red rings, nuclei were excluded). Somatic brightness was calculated by averaging all pixels in each segmented cell. **b-d**. somatic jRGECO1a brightness of labeled neurons in four GP lines and AAV infected mice. Each box indicates the 25th to 75th percentile distribution. Dots inside the boxes indicate the median, and whisker lengths correspond to the 150% of the 25th to 75th percentile distance, or until it touches the last sample position; outliers are marked by dots beyond the whisker range. Colors correspond to brain regions. **b**, Layer 2/3 pyramidal cells (sections from 3–7 mice per line; median, 6; 266–841 cells per brain region; median,684). **c,** Layer 5 pyramidal cells (same number of sections like in **b**; 255–588 cells per brain region; median, 402). **d**, Hippocampal pyramidal cells (sections from 4–6 mice per line; median, 5. 80–913 cells per brain region; median, 303). **e**. Confocal image of GP8.31 fixed tissue (red) counterstained with NeuN (green). **f-h**. Proportion of neurons that are jRGECO1a-positive, estimated by counterstaining with NeuN, corresponding to **b-d**, respectively. (sections from 1 mouse per line; 84–298 cells, median, 160). DG labeling density was high but was not quantified (Results). ALM–anterior-lateral area of the motor cortex, M1 –primary motor cortex, S1 –primary somatosensory cortex, V1 –primary visual cortex, DG–dentate gyrus, CA1, CA3 –areas of the hippocampus.

https://doi.org/10.1371/journal.pone.0205444.g002

and GP8.62 (Fig 2E–2H). GP8.20 exhibited the highest density of neocortical labeling (approximately 60% of neurons); GP8.31 and GP8.58 had 30% labeling density in neocortex; GP8.62 had intermediate labeling density. We note also the relative homogeneity of labeling in the GP8.20 mice compared to GP8.31 mice (Fig 2B and 2C). Hippocampal labeling density was high in the DG for all lines; due to the high cell density in DG, NeuN staining did not allow for separation of individual cells. CA1 labeling density was lower than in the DG, and CA3 labeling density was the lowest, similar to other *Thy1* lines expressing GECIs [6].

Two-photon imaging in the visual cortex

We next tested selected *Thy1*-jRGECO1a lines for imaging activity in layer 2/3 cells of the primary visual cortex (Fig 3A). Four lines were tested: GP8.20, which had the largest proportion of layer 2/3 pyramidal neurons labeled, and GP8.31, GP8.58, and GP8.62, which exhibited different expression patterns. Anesthetized mice were presented with oriented gratings moving in eight different directions (Fig 3A, Methods). Two-photon imaging revealed subsets of jRGECO1a-positive cells showing tuned responses to the stimulus (Fig 3A and 3B). A majority of the responsive neurons were modulated at the 1 Hz temporal frequency of the moving grating. The transgenic lines showed stronger modulation than AAV-jRGECO1a infected mice (Fig 3C).

We analyzed the half-decay time of fluorescence traces after the last response peak during stimulus presentation (Fig 3D, Methods). The averaged half-decay time was faster for the *Thy1*-jRGECO1a lines than for AAV infected mice (2 mice for each Thy1 line; GP8.20, 150±15 ms, n = 69 cells; GP8.31, 135±5, n = 204; GP8.58, 180±15, n = 130; GP8.62, 110±10, n = 119;

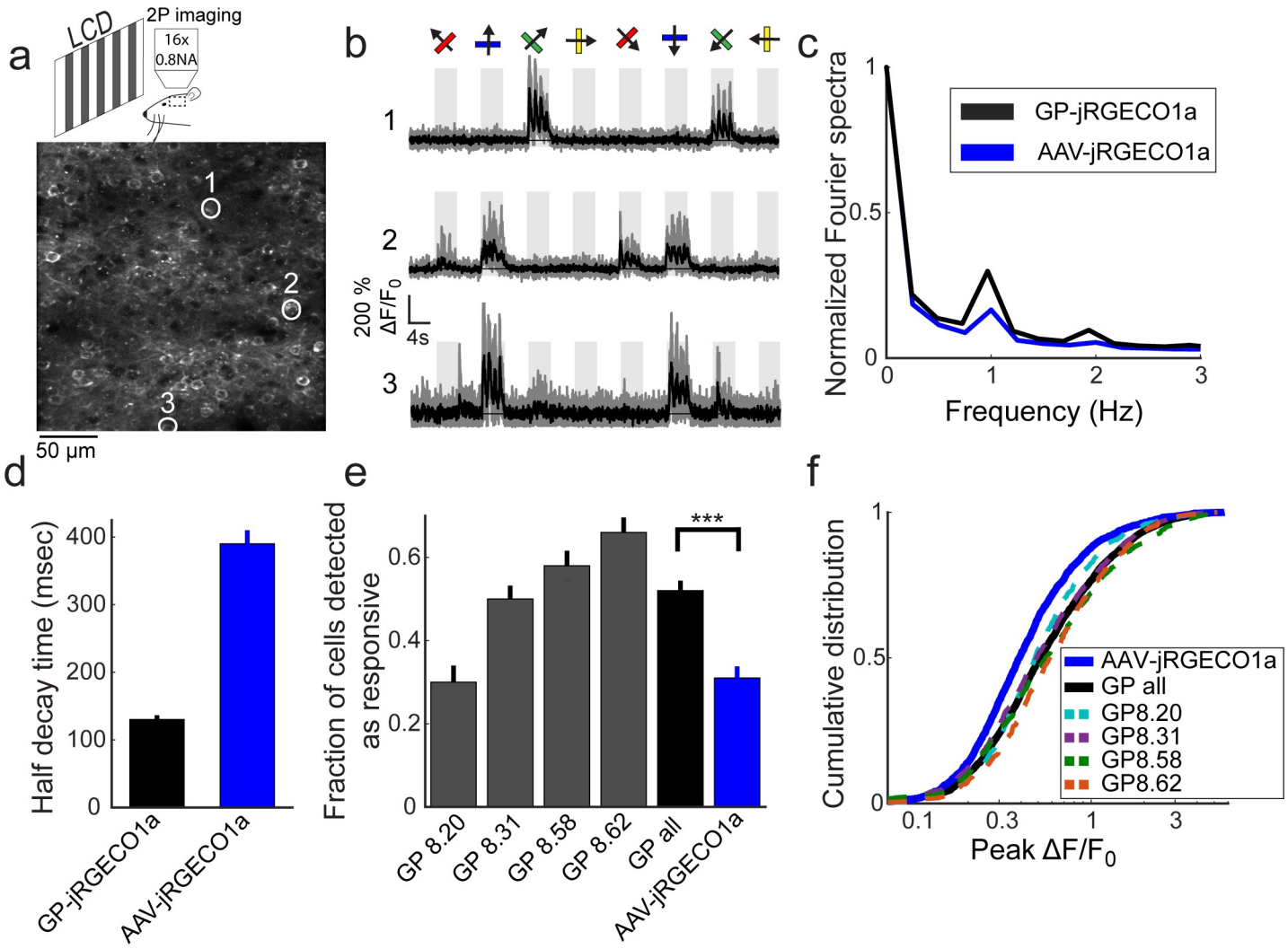

Fig 3. Functional imaging in the primary visual cortex of transgenic mice. a. Schematic of the experimental setup (top), and an image of GP8.31 layer 2/3 cells in the primary visual cortex (bottom, 120 µm under the dura). **b.** Responses of three neurons in GP8.31 mice, indicated by circles in **a,** to drifting grating stimuli. The grating motion directions are indicated by arrows and shown above traces. Single trials (gray) and average of 5 trials (black) are overlaid. The preferred stimulus is the direction evoking the largest response. **c.** Fourier transform of the response to the preferred stimulus (median across all recorded cells) of GP-jRGECO1a and AAV-jRGECO1a. The 1 Hz peak corresponds to the frequency of the drifting grating (AAV-jRGECO1a, 472 significantly responsive neurons from 4 mice; GP-jRGECO1a, 1650 significantly responsive neurons from 8 mice) **d.** Half-decay time (mean ± s.e.) after the last response peak during stimulus presentation (GP-jRGECO1a, n = 522 cells from 8 mice; AAV-jRGECO1a, 395 cells from 4 mice). **e**, Fraction of significant responsive cells (ANOVA test, $p<0.01$). Gray bars, single GP lines (n = 2 mice per line. GP8.20, 709 neurons in 14 FOVs; GP8.31, 1416, 19; GP8.58, 607, 12; GP8.62, 628, 19); black bar, averaged data from all GP lines; blue bar, AAV-jRGECO1a data (n = 4 mice, 1747 neurons in 40 FOVs). ***, $p<0.001$ (Wilcoxon Rank Sum Test). **f**, Distribution of $\Delta F/F_0$ response amplitudes to the preferred stimulus. A right-shifted curve indicates higher response amplitudes. Dashed lines, individual GP lines; black line, compiled data from all GP lines; blue line, AAV-jRGECO1a data (same cells as in **e**). AAV-jRGECO1a data is taken from [4].

https://doi.org/10.1371/journal.pone.0205444.g003

AAV-jRGECO1a data was taken from [4], 390±20, n = 395, 4 mice; mean±s.e.). The half-decay times in the *Thy1*-jRGECO1a lines were in the 150 ms range, close to the kinetics expected for cytoplasmic calcium after an action potential [34]. We note that the faster *Thy1*-jRGECO1a kinetics compared to AAV-jRGECO1a data (Fig 3C and 3D) is consistent with lower expression of the GECI, which leads to weaker calcium buffering, and similar to the reported change with *Thy1*-GCaMP6 lines [6, 35, 36].

Both the fraction of cells that were detected as responsive and the distribution of measured $\Delta F/F_0$ amplitudes were larger in the *Thy1*-jRGECO1a mice compared to AAV infected mice

(Fig 3E and 3F). The fraction of cells detected as responsive (ANOVA test $P<0.01$) was higher for lines with sparser labeling and higher expression level (Fig 2B and 2F) (e.g. GP8.62), and was higher for GP-jRGECO1a than AAV-jRGECO1a (52% vs. 31%, $P<0.001$, Wilcoxson Rank Sum test, Fig 3E). The measured distributions of peak response amplitudes were similar across the GP-jRGECO1a lines, and significantly higher than AAV-jRGECO1a mice ($P<0.001$, Wilcoxon Rank Sum test). The 75-percentile $\Delta F/F_0$ amplitude was 95% for the GP-jRGECO1a mice (3360 cells from 8 mice) and 66% for AAV-jRGECO1a (1605 cells from 4 mice). Finally, the orientation sensitivity index (OSI) of the significantly responsive cells was similar across AAV-jRGECO1a and Thy-jRGECO1a animals, and similar to responses detected with other sensors (S3 Fig).

Widefield imaging of neuronal activity through the intact skull

Compared to blue and green light, red light better penetrates the skull and brain parenchyma because it is much less absorbed by hemoglobin. Absorption by hemoglobin drops off rapidly with increasing wavelength around 590 nm [37]. As a result, the vasculature provides relatively little contrast when viewed through a red (630/75 nm) filter (Fig 4A) compared to a yellow (575/40 nm) filter (Fig 4C). In addition, red light is scattered less compared to light with shorter wavelengths [38]. We reasoned that imaging jRGECO1a should be possible through the skull with relatively little hemodynamic artifact [39].

We imaged activity in the visual cortex through the intact skull (Methods), while the awake mouse was passively watching a checkerboard drifting across its visual field. Fluorescence responses were on the order of 10–15%. The locations of the evoked activity corresponded to the position of the stimulus (Fig 4B). The resulting retinotopic maps (Fig 4C) show a smooth gradient in the primary visual area; as expected, the gradient reverses at the boundaries between the primary visual cortex and higher visual areas [32].

Two-photon imaging of light-evoked responses in the retina

Evaluation of jRGECO1a expression levels in the retina, based on confocal imaging of fixed tissue, identified two *Thy1*-jRGECO1a lines for the study of ganglion cell responses (GP8.5 and GP8.58) (Fig 5A). Retinae of mice from both lines showed apparently adequate transgene expression levels in multiple ganglion cell types, based on soma size and soma distribution density of the labeled cells. We tested the feasibility of imaging light-evoked fluorescence responses in the whole-mount retina *in vitro* in line GP8.5. A contrast-modulated spot (350 μm diameter, 100% Michelson contrast, 1Hz) evoked robust fluorescence response in jRGECO1a-expressing ganglion cell somata (Fig 5A). Responses included ON, OFF, and ON-OFF type responses (Fig 5B), confirming jRGECO1a was expressed in multiple ganglion cell types. Response amplitude in the majority of cells peaked around 1.5 $\Delta F/F_0$ (Fig 5C). Additional tests using directional motion stimuli (drifting square wave gratings) showed direction-tuned responses in a subset of labeled ganglion cells (Fig 5D and 5E). These results demonstrate that line GP8.5 is useful for the study of neural mechanisms underlying direction selectivity, for example, in conjunction with existing green-emitting calcium or glutamate sensor proteins [13, 40].

Discussion

We generated multiple transgenic mouse lines with stable and reproducible expression of jRGECO1a under the *Thy1* promoter ('*Thy1*-jRGECO1a' lines). Each line has a unique expression pattern in the brain, which is the result of random integration of the transgene cassette into the founder genome, reflecting the known chromosomal position effect sensitivity of the

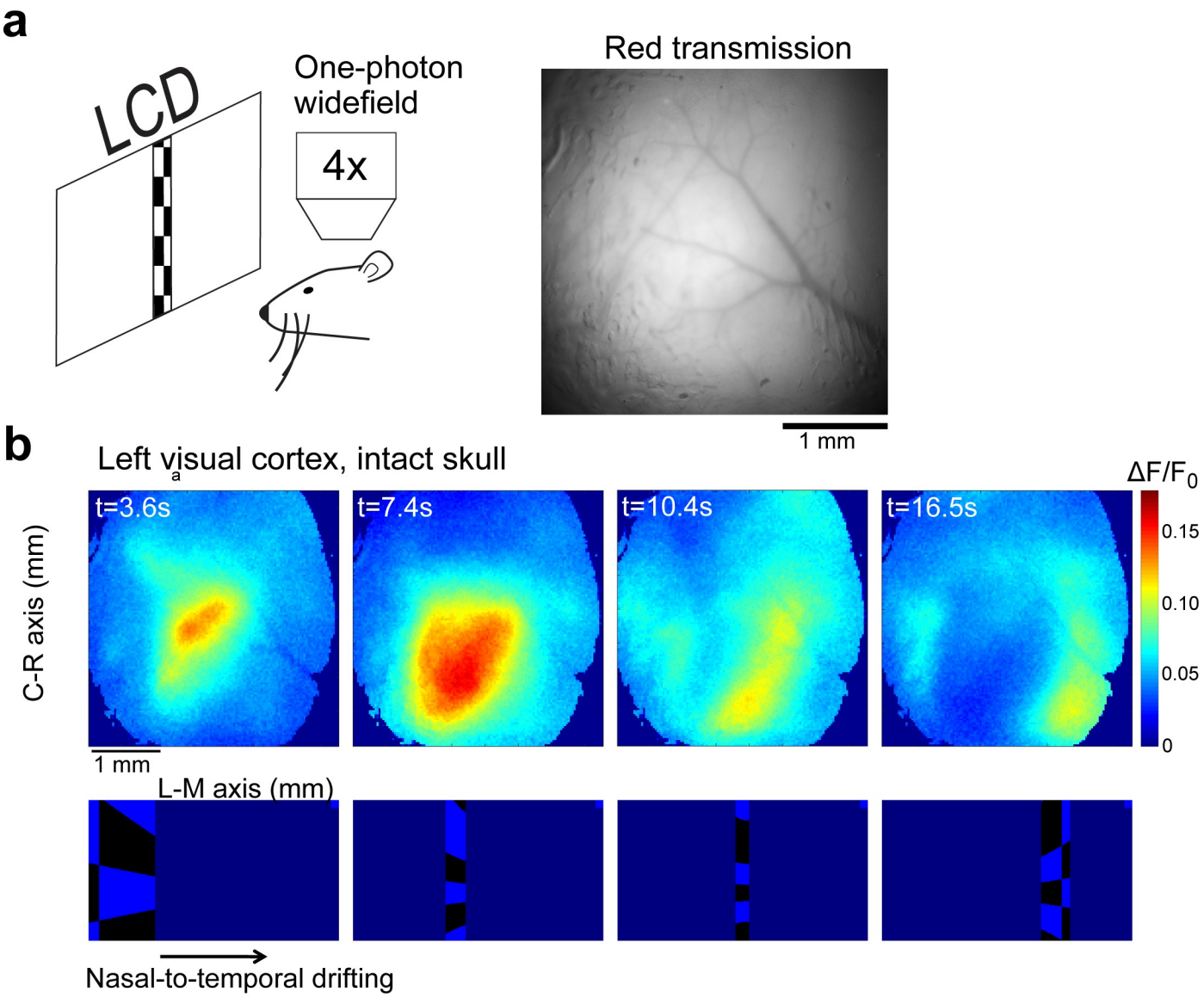

Fig 4. Widefield fluorescence imaging through the intact skull. a, Schematic of widefield imaging and an image of the brain through the intact skull of a 6-weeks old GP8.20 mouse, taken with a red filter set (585 nm dichroic; 630/75 nm emission bandpass filter). **b**. A typical time-lapse sequence capturing activity in the visual cortex (top) elicited by a drifting checkerboard stimulus (bottom) (averaged over 20 stimulus repetitions). Note that the cortical activity splits into two gradients, corresponding to the primary visual cortex and the lateral visual cortex (same mouse as in **a**). **c**. Retinotopy maps superimposed on the cortical surface acquired by yellow emission filter (550nm dichroic; 575/40nm emission bandpass filter) to enhance the contrast of blood vessels. The degree of transparency was set according to the normalized amplitude of the visual response (stronger response → lower transparency, same mouse as in **a**).

https://doi.org/10.1371/journal.pone.0205444.g004

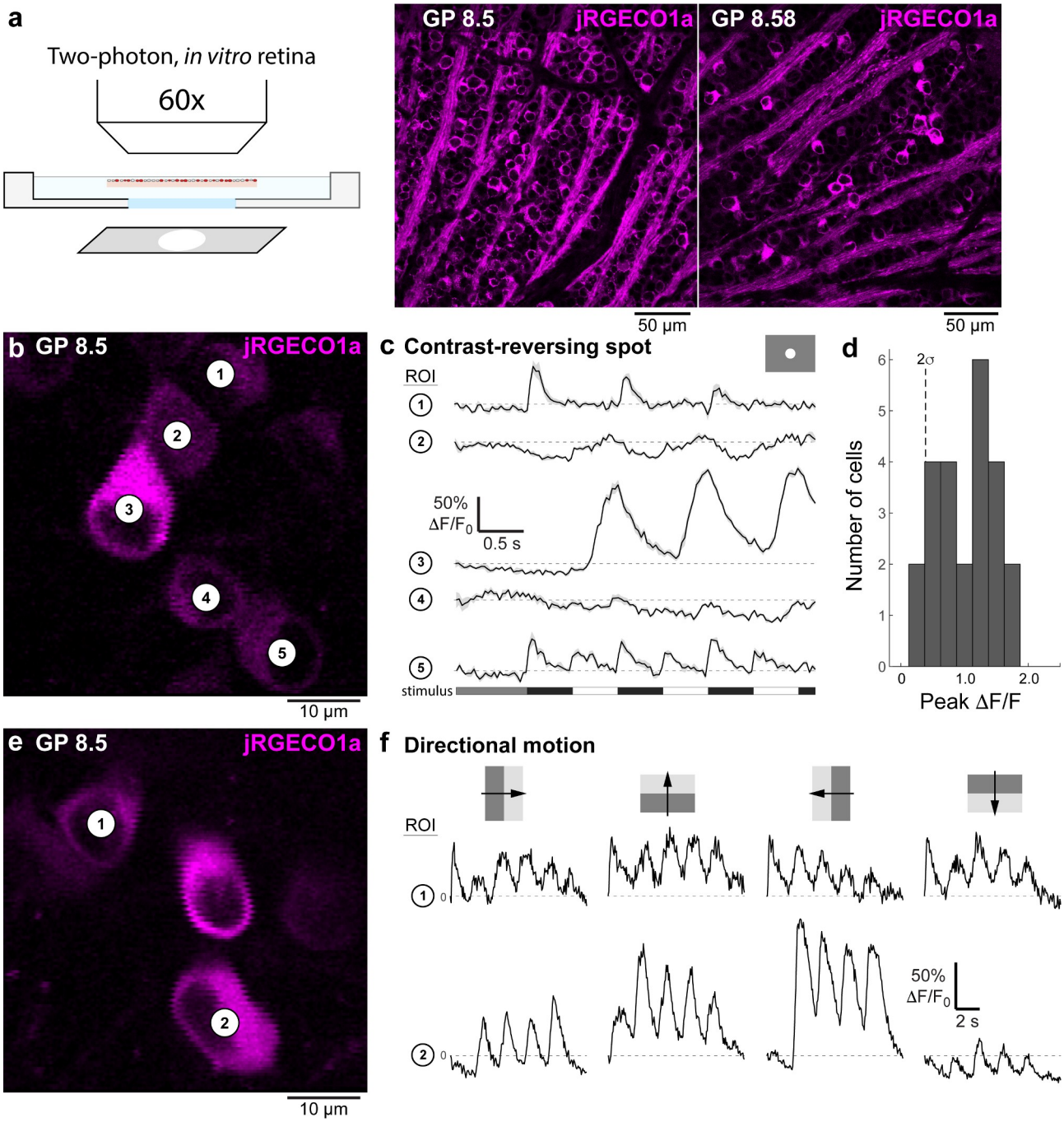

Fig 5. Imaging fluorescence responses of functionally diverse ganglion cell populations in the retina. a, Schematic of the experimental setup (left), and confocal microscopy fluorescence images of retinae taken from GP8.5 and GP8.58 mice (right). **b,** Two-photon fluorescence image of jRGECO1a-expressing ganglion cells in a whole-mount retina, *in vitro* (GP8.5). **c,** Visually-evoked fluorescence responses of the cells indicated in panel **b** to a contrast-modulated 350 µm diameter spot (upper right inset). Fluorescence responses were measured in regions of interest (ROIs), defined as the perimeter of each cells' soma. Stimulus time course shown at bottom (see Methods for details). The labeled ganglion cell population in the GP 8.5 line includes 'OFF' types (e.g., cell 1), 'ON' types (e.g., cell 3), and ON-OFF types (e.g., cell 5). **d,** Histogram of response amplitudes across the recorded ganglion cell population (n = 24). Dashed line indicates two standard deviations of the trial-to-trial variability at baseline (first 1s of the response). **e,** As in **b**, different retinal area. **f,** Fluorescence responses of the two cells indicated in panel **e** during stimulation with oriented drifting gratings (top; grating contrast 100% Michelson; size 500 x 500 µm; wavelength 500 nm; temporal frequency 0.5 Hz). Traces show examples of a non-direction tuned cell (cell 1) and a direction tuned cell (cell 2).

https://doi.org/10.1371/journal.pone.0205444.g005

Thy1 promoter [6, 21, 26]. In each *Thy1*-jRGECO1a line, expression was distributed across numerous neurons and multiple brain regions. Expression levels were well-matched to cellular functional imaging experiments *in vivo*. The sensitivity and kinetics of jRGECO1a make the *Thy1*-jRGECO1a mice a useful tool for high-sensitivity, long-term *in vivo* imaging of neural activity in large neuronal populations. In some cell types, the *Thy1* promoter can drive expression early during postnatal life [26]. Therefore, *Thy1* transgenic mice may facilitate studies in developing mice.

Expression levels in neocortex and hippocampus of *Thy1*-jRGECO1a mice were slightly lower compared to after AAV infection (Fig 2). No signs of cytomorbidity (*e.g.* nuclear filling of cells) was observed in any of the *Thy1*-jRGECO1a transgenic lines. However, jRGECO1a accumulates in lysosomes in these lines, which has previously been observed in AAV-jRGECO1a experiments [4]. The resulting background fluorescence can degrade the signal-to-noise ratio of functional signals. Similarly, green fluorescence indicative of immature jRGECO1a was also detected.

Four *Thy1*-jRGECO1a lines were tested using two-photon imaging of layer 2/3 V1 neurons in anesthetized mice. We observed robust signals with faster kinetics, compared to AAV-jRGECO1a signals (Fig 3C-3F). The enhanced kinetics are consistent with lower cytoplasmic concentrations of jRGECO1a in the *Thy1*-jRGECO1a mice (Fig 2B–2D) and weaker calcium buffering by the indicator [35, 36]. The enhanced sensitivity for detection of neural activity in the transgenic lines over AAV-infected mice remains unexplained, but may involve healthier tissue in the *Thy1*-jRGECO1a transgenic mice.

Widefield imaging of *Thy1*-jRGECO1a cortical activity thorough the intact skull (Fig 4) provides advantages compared to both AAV-mediated expression and transgenic mice expressing green GECIs. Transgenic expression provides labeling across the cortex without surgical interventions. Moreover, hemoglobin absorbs red fluorescence less than green fluorescence [37]. Therefore, hemodynamics is less likely to confound measurements of neural activity with *Thy1*-jRGECO1a mice compared to transgenic mice expressing GCaMP6 [39].

Thy1-jRGECO1a mice have several limitations. Similar to other *Thy1* transgenic mice, *Thy1*-jRGECO1a mice show mosaic expression, unevenly distributed across different brain regions and cortical layers. The *Thy1* promoter drives expression mostly in projection neurons, but the detailed cell types remain to be determined. Other brain cell types, including GABAergic neurons and glia, are generally not accessible using this strategy.

Supporting information

S1 Fig. Similar labeling pattern across different mice from the same line. Confocal images of coronal sections from four different GP8.58 mice, taken from the first and second generations of this line (F1 and F2 respectively), show similar labeling patterns.
(TIF)

S2 Fig. Comparison of AAV and *Thy1*-transgenic labeling patterns. Typical labeling patterns of AAV-mediated expression (left) and *Thy1*-transgenic expression (GP8.20, right) are shown. AAV-mediated expression is localized around the injection site and exhibits large variability in fluorescence protein expression level. The *Thy1*-transgenic expression is generally lower than what achieved with AAV but is more uniform and stable over longer times. Magenta lines indicate the location of labeled L4 cells.
(TIF)

S3 Fig. Comparison of orientation selectivity index (OSI). OSI indicates the tuning level of a cell to a specific orientation of a drifting grating stimulus. The similar distribution of OSI

values for *Thy1*-jRGECO1a and AAV-jRGECO1a, showed in panel **a**, and summarized in panel **b**, indicates that the tuning of the measured cells was not disturbed (*Thy1*-jRGECO1a, 1725 cells from 8 mice; AAV-jRGECO1a, 472 cells from 4 mice).
(TIF)

S1 Data. Widefield images of all characterized GP lines. Images of all characterized GP lines were taken using a slide scanner (Methods). All imaging conditions were kept identical, except for lines GP8.20, GP8.31, GP8.58, and GP.8.62, where the light intensity was reduced to 1/3 of its level with the other lines. Sections are organized from rostral to caudal on the slides, each slide direction is from top to bottom, and the slides are organized from left to right.
(PDF)

Acknowledgments

This study was part of the GENIE project at HHMI Janelia Research Campus (https://www.janelia.org/project-team/genie). We thank Eric Schreiter, Nelson Spruston for comments on the manuscript, Jared Rouchard, Anne Kuszpit, and Kendra Morris for surgical support, and GENIE project team members for discussions.

Author Contributions

Conceptualization: Bart G. Borghuis, Douglas S. Kim, Karel Svoboda.

Formal analysis: Hod Dana, Ondrej Novak, Bart G. Borghuis, Douglas S. Kim.

Investigation: Hod Dana, Ondrej Novak, Michael Guardado-Montesino, James W. Fransen, Amy Hu, Bart G. Borghuis, Caiying Guo, Douglas S. Kim.

Methodology: Hod Dana, Douglas S. Kim, Karel Svoboda.

Project administration: Douglas S. Kim.

Resources: Caiying Guo.

Supervision: Bart G. Borghuis, Douglas S. Kim, Karel Svoboda.

Writing – original draft: Hod Dana, Ondrej Novak, Bart G. Borghuis, Douglas S. Kim.

Writing – review & editing: Hod Dana, Bart G. Borghuis, Douglas S. Kim, Karel Svoboda.

References

1. Sofroniew NJ, Flickinger D, King J, Svoboda K. A large field of view two-photon mesoscope with subcellular resolution for in vivo imaging. Elife. 2016; 5. https://doi.org/10.7554/eLife.14472 PMID: 27300105.
2. Peron SP, Freeman J, Iyer V, Guo C, Svoboda K. A Cellular Resolution Map of Barrel Cortex Activity during Tactile Behavior. Neuron. 2015; 86(3):783–99. https://doi.org/10.1016/j.neuron.2015.03.027 PMID: 25913859.
3. Kim TH, Zhang Y, Lecoq J, Jung JC, Li J, Zeng H, et al. Long-Term optical access to an estimated one million neurons in the live mouse cortex. Cell reports. 2016; 17(12):3385–94. https://doi.org/10.1016/j.celrep.2016.12.004 PMID: 28009304
4. Dana H, Mohar B, Sun Y, Narayan S, Gordus A, Hasseman JP, et al. Sensitive red protein calcium indicators for imaging neural activity. Elife. 2016; 5. https://doi.org/10.7554/eLife.12727 PMID: 27011354; PubMed Central PMCID: PMCPMC4846379.
5. Sun Y, Nern A, Franconville R, Dana H, Schreiter ER, Looger LL, et al. Neural signatures of dynamic stimulus selection in Drosophila. Nature Neuroscience. 2017.
6. Dana H, Chen T-W, Hu A, Shields BC, Guo C, Looger L, et al. Thy1-GCaMP6 Transgenic Mice for Neuronal Population Imaging In Vivo. PloS ONE. 2014; 9(9):e108697. https://doi.org/10.1371/journal.pone.0108697 PMID: 25250714

7. Madisen L, Garner AR, Shimaoka D, Chuong AS, Klapoetke NC, Li L, et al. Transgenic mice for intersectional targeting of neural sensors and effectors with high specificity and performance. Neuron. 2015; 85(5):942–58. https://doi.org/10.1016/j.neuron.2015.02.022 PMID: 25741722; PubMed Central PMCID: PMC4365051.
8. Wekselblatt JB, Flister ED, Piscopo DM, Niell CM. Large-scale imaging of cortical dynamics during sensory perception and behavior. Journal of Neurophysiology. 2016; 115(6):2852–66. https://doi.org/10.1152/jn.01056.2015 PMID: 26912600.
9. Huber D, Gutnisky DA, Peron S, O'Connor DH, Wiegert JS, Tian L, et al. Multiple dynamic representations in the motor cortex during sensorimotor learning. Nature. 2012; 484(7395):473–8. Epub 2012/04/28. https://doi.org/10.1038/nature11039 PMID: 22538608.
10. Akerboom J, Rivera JD, Guilbe MM, Malave EC, Hernandez HH, Tian L, et al. Crystal structures of the GCaMP calcium sensor reveal the mechanism of fluorescence signal change and aid rational design. J Biol Chem. 2009; 284(10):6455–64. https://doi.org/10.1074/jbc.M807657200 PMID: 19098007.
11. Zariwala HA, Borghuis BG, Hoogland TM, Madisen L, Tian L, De Zeeuw CI, et al. A Cre-dependent GCaMP3 reporter mouse for neuronal imaging in vivo. The Journal of Neuroscience. 2012; 32(9):3131–41. https://doi.org/10.1523/JNEUROSCI.4469-11.2012 PMID: 22378886
12. Tian L, Hires SA, Mao T, Huber D, Chiappe ME, Chalasani SH, et al. Imaging neural activity in worms, flies and mice with improved GCaMP calcium indicators. Nat Methods. 2009; 6(12):875–81. Epub 2009/11/10. https://doi.org/10.1038/nmeth.1398 PMID: 19898485.
13. Chen TW, Wardill TJ, Sun Y, Pulver SR, Renninger SL, Baohan A, et al. Ultrasensitive fluorescent proteins for imaging neuronal activity. Nature. 2013; 499(7458):295–300. Epub 2013/07/23. https://doi.org/10.1038/nature12354 PMID: 23868258; PubMed Central PMCID: PMC3777791.
14. Heim N, Garaschuk O, Friedrich MW, Mank M, Milos RI, Kovalchuk Y, et al. Improved calcium imaging in transgenic mice expressing a troponin C–based biosensor. Nature Methods. 2007; 4(2):127–9. https://doi.org/10.1038/nmeth1009 PMID: 17259991
15. Direnberger S, Mues M, Micale V, Wotjak CT, Dietzel S, Schubert M, et al. Biocompatibility of a genetically encoded calcium indicator in a transgenic mouse model. Nat Commun. 2012; 3:1031. https://doi.org/10.1038/ncomms2035 PMID: 22929788
16. Hasan MT, Friedrich RW, Euler T, Larkum ME, Giese GG, Both M, et al. Functional Fluorescent Ca(2+) Indicator Proteins in Transgenic Mice under TET Control. PLoS Biol. 2004; 2(6):E163. https://doi.org/10.1371/journal.pbio.0020163 PMID: 15208716.
17. Díez-García J, Matsushita S, Mutoh H, Nakai J, Ohkura M, Yokoyama J, et al. Activation of cerebellar parallel fibers monitored in transgenic mice expressing a fluorescent Ca2+ indicator protein. European Journal of Neuroscience. 2005; 22(3):627–35. https://doi.org/10.1111/j.1460-9568.2005.04250.x PMID: 16101744
18. Tallini YN, Ohkura M, Choi BR, Ji G, Imoto K, Doran R, et al. Imaging cellular signals in the heart in vivo: Cardiac expression of the high-signal Ca2+ indicator GCaMP2. Proc Natl Acad Sci U S A. 2006; 103(12):4753–8. https://doi.org/10.1073/pnas.0509378103 PMID: 16537386.
19. Tallini YN, Brekke JF, Shui B, Doran R, Hwang SM, Nakai J, et al. Propagated endothelial Ca2+ waves and arteriolar dilation in vivo: measurements in Cx40BAC GCaMP2 transgenic mice. Circ Res. 2007; 101(12):1300–9. Epub 2007/10/13. https://doi.org/10.1161/CIRCRESAHA.107.149484 PMID: 17932328.
20. Atkin SD, Patel S, Kocharyan A, Holtzclaw LA, Weerth SH, Schram V, et al. Transgenic mice expressing a cameleon fluorescent Ca2+ indicator in astrocytes and Schwann cells allow study of glial cell Ca2+ signals in situ and in vivo. Journal of neuroscience methods. 2009; 181(2):212–26. Epub 2009/05/21. https://doi.org/10.1016/j.jneumeth.2009.05.006 PMID: 19454294; PubMed Central PMCID: PMC3142666.
21. Chen Q, Cichon J, Wang W, Qiu L, Lee S-JR, Campbell NR, et al. Imaging Neural Activity Using Thy1-GCaMP Transgenic Mice. Neuron. 2012; 76(2):297–308. https://doi.org/10.1016/j.neuron.2012.07.011 PMID: 23083733
22. Daigle TL, Madisen L, Hage TA, Valley MT, Knoblich U, Larsen RS, et al. A suite of transgenic driver and reporter mouse lines with enhanced brain cell type targeting and functionality. bioRxiv. 2017. https://doi.org/10.1101/224881
23. Bethge P, Carta S, Lorenzo DA, Egolf L, Goniotaki D, Madisen L, et al. An R-CaMP1.07 reporter mouse for cell-type-specific expression of a sensitive red fluorescent calcium indicator. PLOS ONE. 2017; 12(6):e0179460. https://doi.org/10.1371/journal.pone.0179460 PMID: 28640817
24. Chen TW, Li N, Daie K, Svoboda K. A Map of Anticipatory Activity in Mouse Motor Cortex. Neuron. 2017; 94(4):866–79 e4. https://doi.org/10.1016/j.neuron.2017.05.005 PMID: 28521137.
25. Caroni P. Overexpression of growth-associated proteins in the neurons of adult transgenic mice. J Neurosci Methods. 1997; 71(1):3–9. PMID: 9125370.

26. Feng G, Mellor RH, Bernstein M, Keller-Peck C, Nguyen QT, Wallace M, et al. Imaging neuronal subsets in transgenic mice expressing multiple spectral variants of GFP. Neuron. 2000; 28(1):41–51. PMID: 11086982.

27. Behringer R, Gertsenstein M, Vintersten Nagy K, Nagy A. Manipulating the Mouse Embryo: A Laboratory Manual. Fourth edition ed. Cold Spring Harbor, NY, USA: Cold Spring Harbor Laboratory Press; 2013.

28. Donello JE, Loeb JE, Hope TJ. Woodchuck hepatitis virus contains a tripartite posttranscriptional regulatory element. Journal of Virology. 1998; 72(6):5085–92. PMID: 9573279

29. Loeb JE, Cordier WS, Harris ME, Weitzman MD, Hope TJ. Enhanced expression of transgenes from adeno-associated virus vectors with the woodchuck hepatitis virus posttranscriptional regulatory element: implications for gene therapy. Human gene therapy. 1999; 10(14):2295–305. https://doi.org/10.1089/10430349950016942 PMID: 10515449

30. Wolf HK, Buslei R, Schmidt-Kastner R, Schmidt-Kastner PK, Pietsch T, Wiestler OD, et al. NeuN: a useful neuronal marker for diagnostic histopathology. Journal of Histochemistry & Cytochemistry. 1996; 44 (10):1167–71.

31. Guo ZV, Li N, Huber D, Ophir E, Gutnisky DA, Ting JT, et al. Flow of cortical activity underlying a tactile decision in mice. Neuron. 2014; 81(1):179–94. Epub 2013/12/19. https://doi.org/10.1016/j.neuron.2013.10.020 PMID: 24361077.

32. Zhuang J, Ng L, Williams D, Valley M, Li Y, Garrett M, et al. An extended retinotopic map of mouse cortex. eLife [Internet]. 2017 2017/01//; 6.

33. Borghuis BG, Marvin JS, Looger LL, Demb JB. Two-photon imaging of nonlinear glutamate release dynamics at bipolar cell synapses in the mouse retina. Journal of Neuroscience. 2013; 33(27):10972–85. https://doi.org/10.1523/JNEUROSCI.1241-13.2013 PMID: 23825403

34. Sabatini BL, Oertner TG, Svoboda K. The life cycle of Ca(2+) ions in dendritic spines. Neuron. 2002; 33 (3):439–52. Epub 2002/02/08. https://doi.org/S0896627302005731 [pii]. PMID: 11832230.

35. Helmchen F, Imoto K, Sakmann B. Ca^{2+} buffering and action potential-evoked Ca^{2+} signaling in dendrites of pyramidal neurons. Biophys J. 1996; 70:1069–81. https://doi.org/10.1016/S0006-3495(96)79653-4 PMID: 8789126

36. Hires SA, Tian L, Looger LL. Reporting neural activity with genetically encoded calcium indicators. Brain Cell Biol. 2008; 36(1–4):69–86. https://doi.org/10.1007/s11068-008-9029-4 PMID: 18941901.

37. Svoboda K, Block SM. Biological applications of optical forces. Ann Rev of Biophys and Biomol Struct. 1994; 23:247–85.

38. Jacques SL. Optical properties of biological tissues: a review. Physics in Medicine & Biology. 2013; 58 (11):R37.

39. Malonek D, Grinvald A. Interactions Between Electrical Activity and Cortical Microcirculation Revealed by Imaging Spectroscopy: Implications for Functional Brain Mapping. Science. 1996; 272(5261):551–4. https://doi.org/10.1126/science.272.5261.551 PMID: 8614805

40. Marvin JS, Borghuis BG, Tian L, Cichon J, Harnett MT, Akerboom J, et al. An optimized fluorescent probe for visualizing glutamate neurotransmission. Nat Methods. 2013; 10(2):162–70. https://doi.org/10.1038/nmeth.2333 PMID: 23314171; PubMed Central PMCID: PMCPMC4469972.